Journal of Applied Mechanics and Technical Physics, Vol. 43, No. 6, pp. 877–887, 2002

MATHEMATICAL SIMULATION OF DUST LIFTING FROM THE SURFACE

A. V. Fedorov,[1] **N. N. Fedorova,**[1]
I. A. Fedorchenko,[2] **and V. M. Fomin**[3]

UDC 532.529

Results of numerical simulation of the shock wave passing along a dusty layer are presented; the simulation was performed under the one-temperature, one-velocity assumption. It is shown that a system of compression and expansion waves is formed inside the layer, and these waves are successively reflected from the external boundary and solid wall. Regular and irregular reflections of the leading shock wave from the solid wall with different scenarios of instability evolution on the layer edge are described. Possible mechanisms of particle lifting from the surface are described.

Introduction. Problems of explosion and fire safety in dusty industries have attracted the researchers' attention for decades. A large number of experimental and theoretical works have been fulfilled. Nevertheless, the mechanisms of heterogeneous detonation of dusty suspensions have not been identified, and there is no mathematical model taking into account all factors of this complicated process.

Emergence of an explosion in a dusty atmosphere, for instance, in a coal mine, can have the following scheme. Exhausted mines usually contain coal dust, which is unstable to certain force actions, e.g., to the action of a shock wave (SW) initiated in some technologies. The SW action creates a flow in the mine atmosphere impinging on the dusty layer with a high velocity, which leads to lifting of small coal particles and to the formation of a coal–gas mixture. A rather high temperature of air can lead to ignition, combustion, and explosion of the dusty cloud. Thus, one of the main problems in studying the origination of heterogeneous detonation is the physico-mathematical description of mixing of coal particles with a subsonic or supersonic air flow.

The mechanism of formation of a dusty suspension behind transient shock waves was considered in many papers experimentally and theoretically within the framework of the linear theory. In [1–5], the dust-lifting process is explained by the action of a system of compression and expansion waves formed due to successive reflection of the leading shock wave from the solid surface and cloud boundary, which is responsible for evolution of the Kelvin–Helmholtz instability of the contact surface. In addition, lifting of dust particles may be caused by the action of Saffman or Magnus forces, turbulent diffusion, etc. (see the review in [6, 7]).

The objective of the present work is to study numerically the wave processes in a pseudo-liquefied layer with a shock wave sliding along the layer and to explain possible mechanisms of dust-particle lifting.

1. Formulation of the Problem. The flow pattern for the considered two-dimensional unsteady problem of mechanics of heterogeneous media is shown in Fig. 1a. The shock wave moves from left to right over a quiescent gas with parameters $u_0 = 0$, ρ_0, T_0, and p_0. The wave velocity is defined by the shock-wave Mach number $\mathrm{M_s}$: $D = \mathrm{M_s} c_0$ (c_0 is the velocity of sound based on gas parameters ahead of the SW front). On the plate surface, there is a layer of thickness h of a denser ($\rho_0 < \rho_1$) gas, which simulates the gas mixture at the first stage. The layer density is characterized by the dimensionless Atwood number $\mathrm{A} = (\rho_1 - \rho_0)/(\rho_1 + \rho_0)$, where $0 \leqslant \mathrm{A} < 1$. The elevated density of the layer may be caused by the presence of a disperse phase with an initial volume concentration $m_{20} > 0$ or by a lower gas temperature $T_1 < T_0$. The calculations showed that the flow pattern in all these cases is qualitatively identical.

[1]Novosibirsk State University of Architecture and Construction Engineering, Novosibirsk 630008. [2]Novosibirsk State Technical University, Novosibirsk 630092. [3]Institute of Theoretical and Applied Mechanics, Siberian Division, Russian Academy of Sciences, Novosibirsk 630090. Translated from Prikladnaya Mekhanika i Tekhnicheskaya Fizika, Vol. 43, No. 6, pp. 113–125, November–December, 2002. Original article submitted April 29, 2002.

0021-8944/02/4306-0877 $27.00

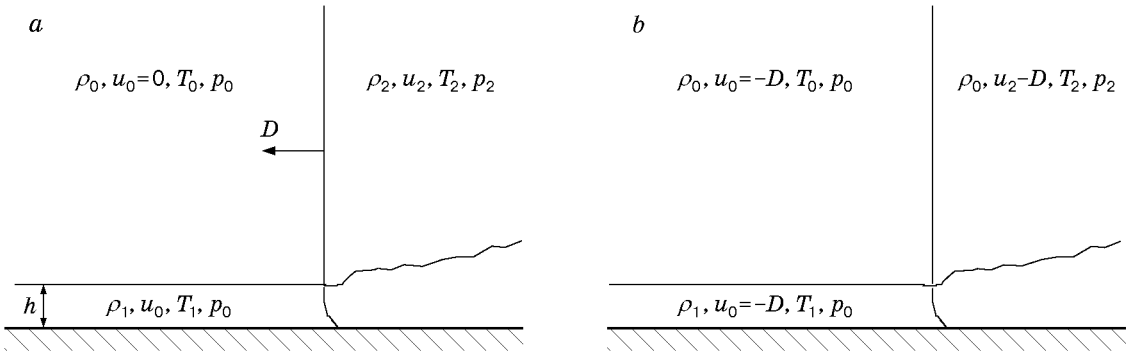

Fig. 1. Calculation scheme of the two-dimensional problem of SW motion along a dense layer in the laboratory coordinate system (a) and in the shock-wave-fixed coordinate system (b).

A flow with a velocity u_2 is formed behind the shock wave in a pure gas; the flow direction coincides with the SW propagation direction. The gas parameter ahead of the SW are $\rho_0 = 1.177$ kg/m^3 and $T_0 = 288$ K. The gas parameters ρ_2, T_2, and u_2 behind the SW at the initial time are calculated from the relations on the normal shock.

In the present calculations, we used an SW-fixed coordinate system (Fig. 1b) where the plate and the gas move from left to right with a velocity D before the shock incidence, and the velocity of the pure gas after the shock is $u_2 - D$.

The calculations were performed within the framework of the one-velocity model of mechanics of heterogeneous media for the following parameters: $h = 5$ mm, $\mathrm{M_s} = 1.6$, 2.0, 2.5, and 3.0, A = 1/5, 1/3, 3/7, 1/2, and 2/3, and initial volume concentration of dust $m_2 = 10^{-3}$, which corresponds to A = 0.385. Coal particles were considered as a disperse material.

2. Mathematical Model and Calculation Technique. The calculation was performed within the framework of the Navier–Stokes equations of a viscous heat-conducting gas

$$\frac{\partial \boldsymbol{Q}}{\partial t} + \frac{\partial \boldsymbol{F}}{\partial x} + \frac{\partial \boldsymbol{G}}{\partial y} = 0,$$

where $\boldsymbol{Q} = (\rho, \rho u, \rho v, \rho E)$ is a column-vector of conservative variables, $\boldsymbol{F} = \boldsymbol{F}_{\mathrm{inv}} - \boldsymbol{F}_{\mathrm{vis}}$ and $\boldsymbol{G} = \boldsymbol{G}_{\mathrm{inv}} - \boldsymbol{G}_{\mathrm{vis}}$ are flux vectors represented as a sum of inviscid and viscid terms:

$$\boldsymbol{F}_{\mathrm{inv}} = \begin{pmatrix} \rho \\ \rho u^2 + p \\ \rho uv \\ \rho Hu \end{pmatrix}, \quad \boldsymbol{G}_{\mathrm{inv}} = \begin{pmatrix} \rho v \\ \rho uv \\ \rho v^2 + p \\ \rho Hv \end{pmatrix}, \quad \boldsymbol{F}_{\mathrm{vis}} = \begin{pmatrix} 0 \\ \tau_{xx} \\ \tau_{xy} \\ f_x \end{pmatrix}, \quad \boldsymbol{G}_{\mathrm{vis}} = \begin{pmatrix} 0 \\ \tau_{xy} \\ \tau_{yy} \\ f_y \end{pmatrix}.$$

The components of the viscous stress tensor may be written as

$$\tau_{xx} = \mu\Big(\frac{4}{3}\frac{\partial u}{\partial x} - \frac{2}{3}\frac{\partial v}{\partial y}\Big), \quad \tau_{xy} = \mu\Big(\frac{\partial u}{\partial y} - \frac{2}{3}\frac{\partial v}{\partial x}\Big), \quad \tau_{yy} = \mu\Big(\frac{4}{3}\frac{\partial v}{\partial y} - \frac{2}{3}\frac{\partial u}{\partial x}\Big),$$

$$f_x = q_x + \tau_{xx}u + \tau_{xy}v, \qquad f_y = q_y + \tau_{xy}u + \tau_{yy}v,$$

and the heat fluxes in the form

$$q_x = \gamma\,\frac{\mu}{\mathrm{Pr_{lam}}}\,\frac{\partial e}{\partial x}, \qquad q_y = \gamma\,\frac{\mu}{\mathrm{Pr_{lam}}}\,\frac{\partial e}{\partial y}, \qquad \mathrm{Pr_{lam}} = 0.723.$$

Here H is the total enthalpy, $\mathrm{Pr_{lam}}$ is the laminar Prandtl number, and μ is the viscosity.

The problem was solved in two approximations. In the first case, as is noted above, the mixture was simulated by a gas with the equation of state $p = (\gamma - 1)\rho e$. It was assumed that the dusty medium is a high-density gas.

In the second approach, the mixture was assumed to be a generalized one-velocity, one-temperature gas within the framework of the model of mechanics of equilibrium heterogeneous media. This model includes a system of conservation laws for a viscous heat-conducting pseudogas, which is supplemented by an equation for the volume concentration of particles:

$$\frac{\partial m_2}{\partial t} + \frac{\partial m_2 u}{\partial x} + \frac{\partial m_2 v}{\partial y} = 0.$$

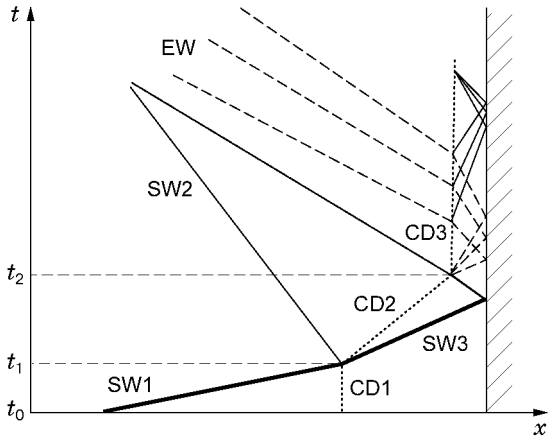

Fig. 2. Wave pattern for the one-dimensional unsteady model problem.

The equation of state of the mixture is

$$p = RT\xi_1\rho/(1 - m_2),$$

where R is the universal gas constant, T is the temperature, $\rho = \rho_1 + \rho_2$ is the density of the mixture, $\xi_1 = \rho_1/\rho = \rho_{11}m_1/\rho$ is the relative mass concentration of air, and ρ_{11} is the true density of air.

The time approximation is performed using a scheme of the unified-algorithm type [8] with a specially chosen stabilizing operator. The use of the method of splitting with regard to spatial variables allows us to divide the problem into four fractional steps at each time step. Each fractional step is implemented by three-point sweeps, which makes the numerical algorithm rather economical.

Convective terms are approximated using a TVD-scheme constructed on the basis of splitting of the inviscid-flux vector with regard to physical processes [9]. Viscous terms are approximated by second-order difference operators on symmetric grid stencils. The calculation method and test calculations are described in detail in [10].

3. One-Dimensional Model Problem. Before solving the problem in the full two-dimensional unsteady formulation, we consider a one-dimensional unsteady problem whose pattern is shown in Fig. 2. The shock wave moves from left to right in a constant-section channel with a closed right end in a vicinity of which a dusty-gas layer is located. The flow parameters are $P = 0.723$, $\rho = 1$, $u = 0$, and $m_2 = 0$ upstream of the SW and $P = 2.04$, $\rho = 2.08$, $u = 0.81$, and $m_2 = 0$ behind the SW. The density, velocity, and pressure were normalized using the following scales: pure gas density ρ_0, velocity of sound ahead of the SW c_0, and the complex $\rho_0 c_0^2$. The objective of the study is to obtain the flow pattern and estimate the parameters of dust lifting caused by propagation of the SW reflected from the rigid wall. The wave pattern of the flow in the plane (x, t) is shown in Fig. 2 (SW1 is the incident shock wave, CD1 is the contact discontinuity (boundary between the dusty and pure gases) whose velocity at the initial moment equals zero, and EW is the expansion wave). At the time t_1, the shock wave interacts with the contact discontinuity separating the pure and dusty gases; as a result, the shock wave is partly reflected (SW2) and partly refracted (SW3) and enters the dense layer. Under the action of the incident shock wave, the layer of particles limited by the contact discontinuity (CD2) acquires a positive velocity, i.e., its compacting occurs. At the time t_2, the reflected shock wave arrives at the contact boundary, another interaction occurs, and this shock wave is partly reflected and partly refracted and enters the pure gas. Since the wave leaves a denser medium and enters a less dense medium, it is reflected from the contact discontinuity as an expansion wave, which is again incident onto the solid wall. As a result of multiple reflection of compression and expansion waves from the contact boundary and solid wall, the pressure becomes equalized, and the velocity of the contact discontinuity (CD3) becomes close to zero again. The layer of the dusty gas occupies an equilibrium position near the solid wall. Nevertheless, the layer thickness may change under the action of compression and expansion waves on the interface boundary.

Thus, the wave pattern in the one-dimensional unsteady model problem is similar to the wave pattern in the two-dimensional problem considered and can be used to study the latter, to explain possible mechanisms of detachment of the dusty layer under the action of internal waves, and to test the calculation technique. We assume that the time when SW3 reflected from the rigid wall arrives at the boundary between the dusty and pure gases corresponds to the moment of dust lifting. Indeed, a reflected expansion wave arises at the contact boundary at this moment, where the particles may obtain acceleration in the direction away from the wall.

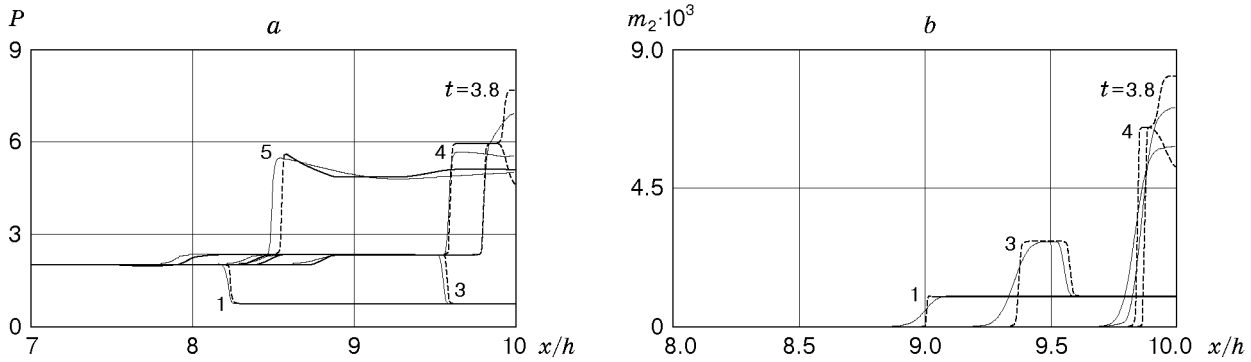

Fig. 3. Distributions of static pressure (a) and particle concentration (b) along the channel, obtained by the CIP method (solid curve) and TVD method (dashed curves).

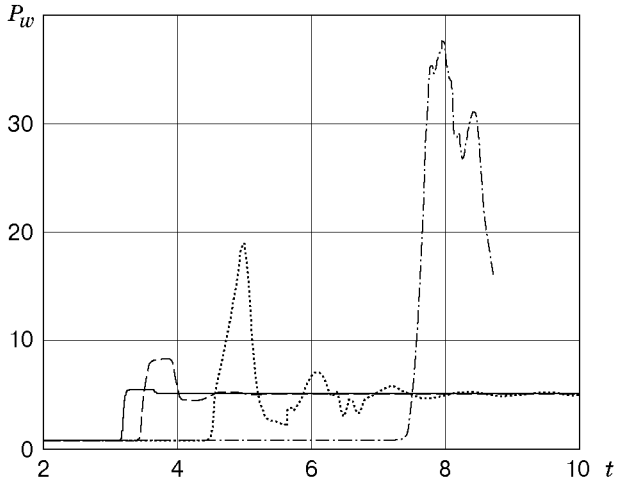

Fig. 4. Static pressure on the end face of the channel versus time for A = 0.067 (solid curve), 0.419 (dashed curve), 0.878 (dotted curve), and 0.986 (dot-and-dashed curve).

This problem was solved in the above-mentioned one-velocity approximation of mechanics of heterogeneous media. The mixture of the gas and particles was assumed to be inviscid and heat-non-conducting, and its motion was described by the Euler equations supplemented by a one-dimensional analog of the equation for the volume concentration of particles and by the equation of state mentioned earlier. In addition to the standard TVD method, the initial-boundary problem was solved using the so-called cubic interpolation propagation (CIP) method proposed in [11], which works well in solving problems with strong contact discontinuities.

Figure 3 shows the distributions of static pressure and volume concentration of particles for $M_s = 1.6$ and $m_{20} = 10^{-3}$, which were obtained in calculations by the TVD method of the third-order approximation with regard to the spatial variable (dashed curves) and by the CIP method (solid curves). It follows from Fig. 3 that both methods describe the above-mentioned wave pattern of the flow rather accurately. Nevertheless, the use of the TVD method yields rather blurred contact boundaries. The CIP method reproduces all wave features of the flow with a high accuracy (and describes the contact boundary rather accurately); in addition, this method allows calculations with rather high initial volume concentrations of particles. Figure 4 shows the static pressure at the channel end face versus time. It follows from Fig. 4 that the wave intensity increases considerably in the layer of particles. In the case of high initial volume concentrations, compression and expansion waves are observed on the end face.

Figure 5 shows the trajectories of the contact boundary separating the pure and dusty gases. Under the action of the shock wave, the dusty layer is considerably compressed; the compression is stronger for high initial concentrations. This can be attributed to the fact that higher concentrations lead to a stronger increase in SW intensity (see Fig. 4). After SW reflection from the wall, insignificant "swelling" of the layer is observed, which

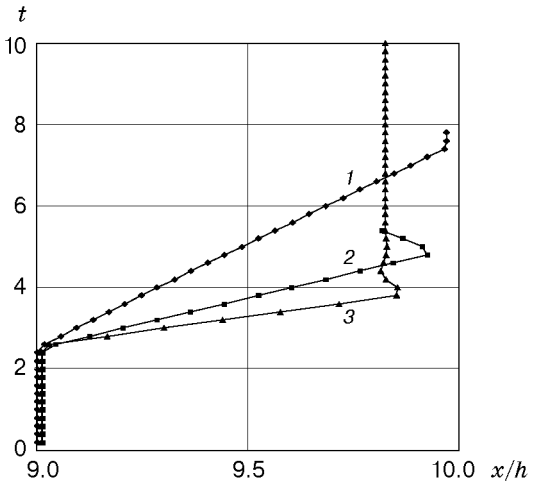

Fig. 5. Trajectories of motion of the contact boundary for $m_2 =$ 0.1 (curve 1), 0.01 (curve 2), and =0.001 (curve 3).

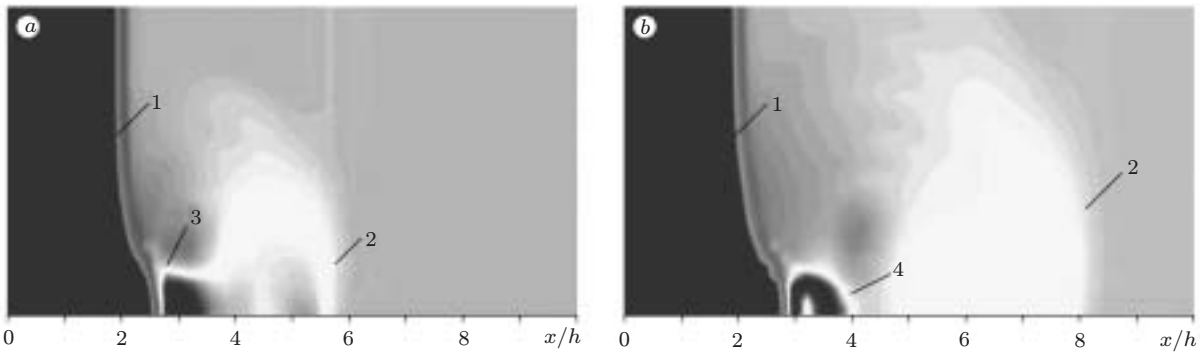

Fig. 6. Static pressure distribution along the plate surface for $t = 12$ (a) and 36 μsec (b): 1) leading SW; 2) compression wave; 3) reflected wave; 4) expansion wave.

corresponds to dust lifting, i.e., it is at this moment that the velocity of the contact discontinuity becomes negative. For values of m_2 corresponding to the curves in Fig. 5, the wave process relaxes rather rapidly to the equilibrium state.

Thus, based on calculations of the one-dimensional unsteady model problem in the approximation of one-velocity mechanics of heterogeneous media, it is shown that the SW incidence onto a dusty layer located near a solid wall leads to a significant increase in SW intensity and to the formation of a system of compression and expansion waves successively reflected from the solid wall and contact surface. These waves change the shape of the contact surface, but their action is insignificant and cannot be used to explain the mechanism of particle lifting in the two-dimensional problem.

4. Calculation Results for the Two-Dimensional Problem. Numerical simulation allowed us to determine and analyze the wave pattern of the flow formed in the vicinity of the shock-wave front. Figures 6 and 7 show the fields of static pressure and density for $M_s = 2$ and $A = 1/3$ at the times $t = 12$ and 36 μsec. At the initial time $t = 0$, the leading SW reaches the edge of the rectangular layer with an elevated density and is partly reflected from it as a low-intensity compression wave (approximately 0.1 atm), which propagates from left to right and rather rapidly leaves the computational domain. In the dense layer adjacent to the solid wall, the front of the leading SW becomes curved. The curved wave is incident onto the plate surface and reflected from it in an irregular manner (see Fig. 6a). Under the action of high pressure arising in the layer of particles loaded by the incident SW, a high-velocity jet of the dusty gas emerges and propagates behind the SW. The boundary between this jet and pure gas is seen in Fig. 7. The curved SW reflected from the plate surface arrives at the contact surface and is reflected from it as an expansion wave (see Fig. 6b), which is again incident onto the plate surface. Then the

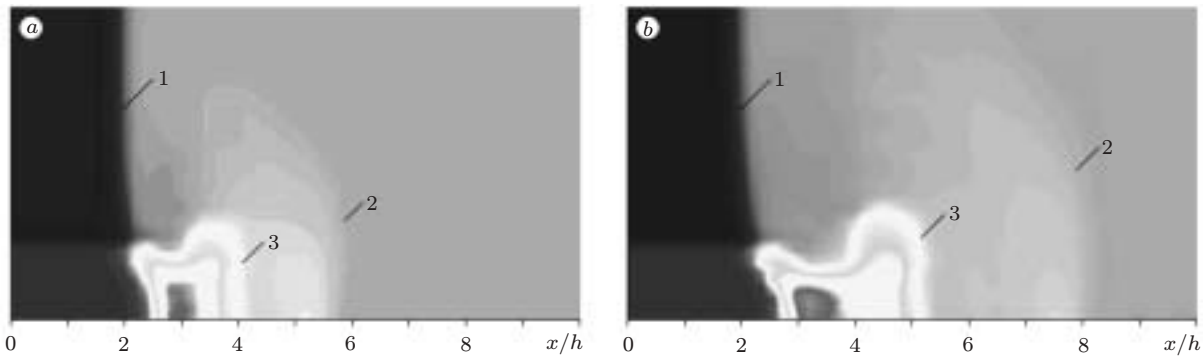

Fig. 7. Density distribution along the plate surface for $t = 12$ (a) and 36 μsec (b); 1) leading SW; 2) compression wave; 3) boundary between pure and dusty gases.

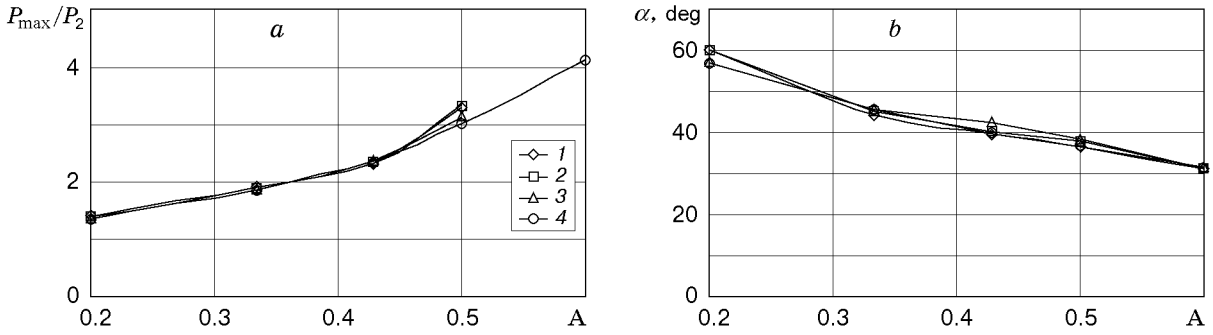

Fig. 8. SW-amplification factor (a) and angle formed by the SW with the surface (b) as functions of the Atwood number for $M_s = 1.6$ (1), 2.0 (2), 2.5 (3), and 3.0 (4).

process is repeated; as a result, a system of compression and expansion waves successively reflected from the plate surface and jet boundary is formed in the layer behind the SW. The wave intensity decreases with distance from the leading SW.

At the initial stage of interaction, a significant increase in SW intensity and curving of the SW front are observed in the dense layer. Figure 8 shows the SW-amplification factor P_{max}/P_2 and angle of inclination of the SW front to the plate surface as functions of the Atwood number for different values of M_s, which were obtained by processing numerical data. As the Atwood number increases, the SW-amplification factor in the dense layer and the angle of deviation of the shock wave from its normal position increase; both parameters are independent of the SW Mach number.

The SW curved inside the dusty layer is reflected from the solid surface. Depending on the SW intensity and initial loading of the flow, either regular or irregular (Mach) reflection can be formed. For low values of A, the shock wave approaches the solid surface at a greater angle than in the case of high values of A. Hence, conditions for irregular and regular SW reflection from the solid wall are formed in the case of low and high Atwood numbers, respectively.

Figure 9 shows the flow patterns for regular and irregular SW reflection. In the case of regular reflection (Fig. 9a), the flow pattern coincides with the wave scheme proposed in [1–5]. Layer compression is observed behind the SW front; a greater change in the layer thickness corresponds to a more intense SW. The leading SW with a curved front arrives at the surface at an angle at which regular SW reflection from the solid wall is observed. The reflected SW approaches the interface between the pure and dusty gases, is partly reflected and partly refracted, and enters the pure gas. Since the shock wave arrives from a denser medium, it is reflected from the contact boundary as an expansion wave. The expansion wave is incident onto the plate surface, is reflected from it, reaches the contact surface again, etc. The wave intensity decreases with distance from the SW front. For weak shock waves, the intensity of internal waves decreases rather rapidly, since the external pressure behind the SW front is rather low, and significant part of the wave energy is released into the ambient medium in each interaction with the contact surface. For strong shock waves with a high pressure behind the front, the relation between the intensities

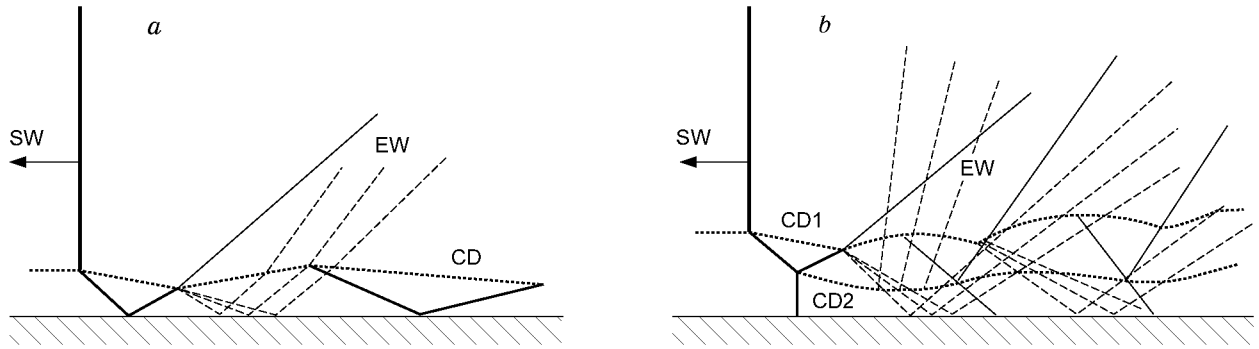

Fig. 9. Flow patterns in the case of regular (a) and irregular (b) SW reflection.

of reflected and transient waves is different, and the waves are observed inside the layer at a rather large distance from the front of the leading SW. The shape of the contact surface changes periodically: the valleys correspond to arrival of compression waves at the contact surface, and the peaks to arrival of expansion waves.

Under the action of internal waves, redistribution of particle concentration inside the layer occurs. The highest density of particles is observed on the wall, and there are maxima in those regions where the compression waves are incident. Thus, the calculation results confirm the formation of a system of compression and expansion waves inside the layer at high Atwood numbers, which was observed experimentally in [1].

In the case of irregular reflection (Fig. 9b), an additional contact discontinuity leaves the triple point; the presence of this discontinuity significantly alters the wave pattern of the flow. Figure 9b shows the triple point formed by the Mach stem and incident and reflected waves, as well as the contact discontinuity (CD2) emanating from the triple point. Downstream from the triple point, the contact surface develops into a jet that forms a denser flow core on which refraction and reflection of internal wave also occur. The internal jet divides the whole layer into two parts, with a separate system of incident and reflected waves in each part. As a result, the length of internal waves becomes significantly smaller than in regular reflection, and their intensity decreases rapidly. In this case, the maximum density is observed in the region of the internal contact surface rather than on the solid surface. In addition, the existence of another system of internal waves in the upper part of the layer leads to rapid development of instability of the external contact boundary.

Figure 10 shows the isolines of static pressure, vertical velocity, and density in the vicinity of the SW for $\mathrm{M_s} = 3$ and $\mathrm{A} = 1/2$. In this case, irregular reflection with a Mach stem height of approximately 1 mm is formed. The picture of density isolines for $10 < X < 15$ contains an additional contact discontinuity emanating from the triple point (point B). One can also see compression and expansion waves reflected from the plate surface and contact boundary. It follows from Fig. 10b that the flow is directed downward behind the curved SW front ($V_{\min} \approx -380$ m/sec), and then it changes its direction to the opposite one, being reflected from the wall. The positive velocity $V_{\max} \approx 150$ m/sec leads to insignificant "swelling" of the layer.

We can assume that the presence of a region with a significant positive vertical velocity behind the leading shock wave will eject large particles present in the flow in the upward direction. Figure 11 compares the results of one-dimensional and two-dimensional calculations with the empirical dependence of the distance from the shock wave to the point where the dust lifting begins on the relative Mach number of the flow behind the SW and layer thickness [12]:

$$\Delta x = 0.17 \mathrm{M}_{\mathrm{rel}}^{2} \sqrt{h}. \tag{1}$$

This formula is transformed to the dependence of the dust-lifting delay $\Delta t = \Delta x / D$ on the Mach number of the leading SW and is plotted in Fig. 11 by the solid curves for $h = 1$ and 5 mm. The open points correspond to the results of one-dimensional calculations where the delay was determined as the time between the moment of SW arrival at the dusty-layer boundary and the moment of arrival of the SW reflected from the wall at the contact surface. The filled points correspond to the results obtained in the two-dimensional formulation for various SW Mach numbers and a layer thickness $h = 5$ mm. The delay was determined by the distance between the SW front and the point of arrival of the reflected SW at the contact surface. At this point, the vertical velocity is positive, and dust particles are ejected upward. It follows from Fig. 11 that the results of one-dimensional calculations for $h = 1$ mm and $m_2 = 10^{-3}$ is in quantitative agreement with the calculation results by formula (1). For $h = 5$ mm,

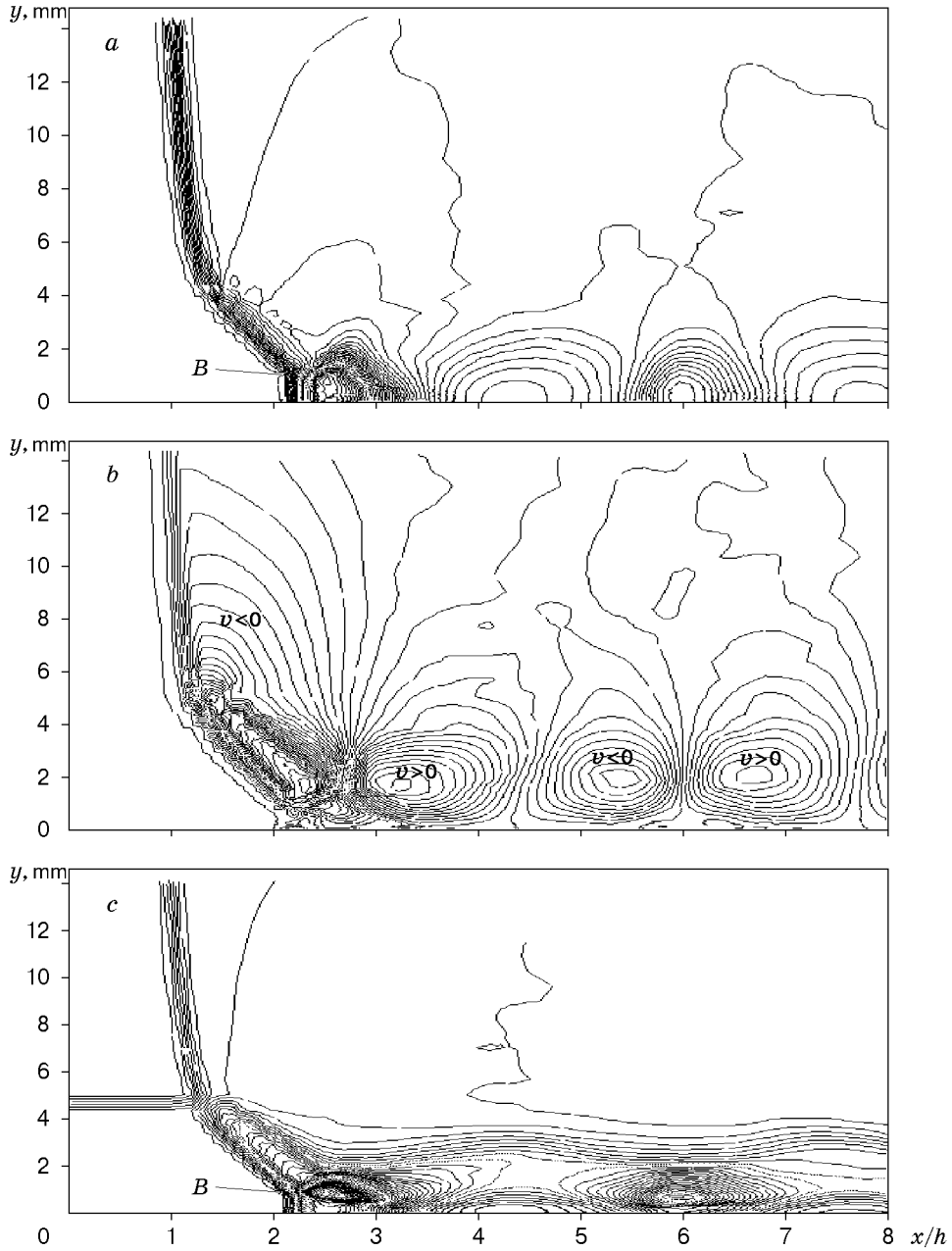

Fig. 10. Isolines of static pressure (a), vertical velocity (b), and density (c) in the vicinity of the SW for $M_s = 3$ and $\rho_1/\rho_0 = 3$ (B is the triple point).

the results of one-dimensional calculations correspond quantitatively to the results of two-dimensional calculations, but the numerical results are only in qualitative agreement with the empirical formula (1). The difference may be caused by the fact that formula (1) does not take into account the initial density of the layer, which (as was shown by one-dimensional and two-dimensional calculations) affects the wave structure. The delay of dust lifting versus the Mach number for different values of the initial dust concentration is plotted by points in Fig. 11. The calculation data yield a correct description of the dependence $\Delta t(M_s)$. It should be noted that $m_2 \approx 0.3$ in the experiments of [12], which is significantly higher than the value used in calculations. Therefore, the results of calculations and experiments can be compared only qualitatively.

Figure 12 shows the Mach stem height calculated as a function of the Atwood number for different values of the SW Mach number. For small values of the SW Mach number M_s, the transition to regular reflection occurs at lower Atwood numbers than for high values of M_s.

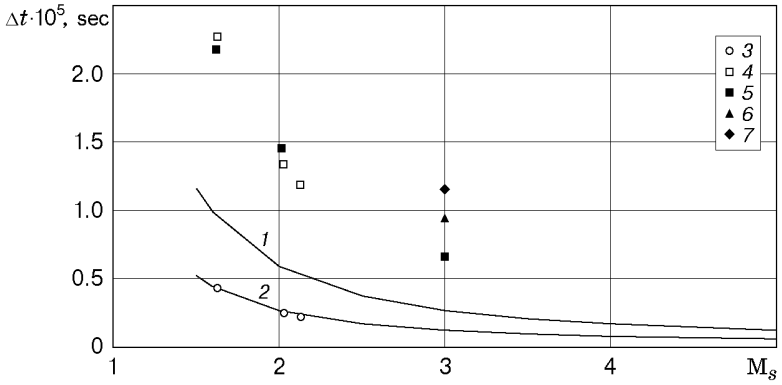

Fig. 11. Delay of dust lifting versus the Mach number: curves 1 and 2 refer to calculations by the empirical formula (1) for $h = 5$ and 1, respectively; the open points refer to one-dimensional calculations for $m_2 = 0.001$ and $h = 1$ (3) and 5 mm (4) and the filled points refer to two-dimensional calculations for $m_2 = 0.0008$ (5), 0.0016 (6), and 0.0024 (7).

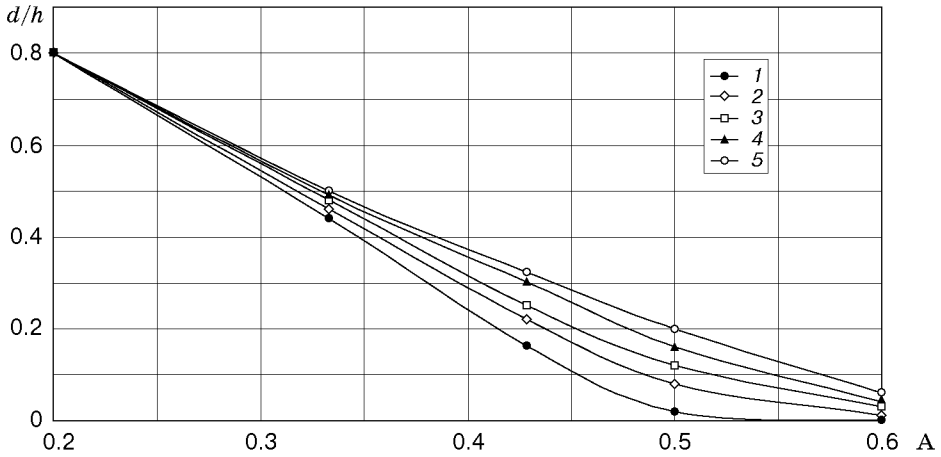

Fig. 12. Mach stem height versus the Atwood number for $M_s = 1.6$ (1), 2.0 (2), 2.5 (3), 3.0 (4), and 4.0 (5).

Figure 13 shows the pressure distribution along the plate surface for $M_s = 3$ and different Atwood numbers. In the case of regular reflection observed at high Atwood numbers, the SW intensity significantly increases, and the internal waves are observed at a considerable distance from the front. In the case of irregular reflection ($A = 1/3$), the wave intensity is significantly smaller, and the waves are rapidly damped. Beginning from the distance $x/h = 15$, however, static pressure perturbations are observed on the plate surface, which are a consequence of the Kelvin–Helmholtz instability developing at the interface of the pure and dusty gases.

Figure 14 shows the density fields for $M_s = 2$ and $A = 1/3$ for different times. Compression and expansion waves reflected inside the dense layer do not cause significant changes in the layer thickness. Considerable lifting of particles from the surface is caused by an unsteady vortex structure into which the leading front of the dusty gas jet is "swirled." When the leading front of the jet leaves the computational domain, the pattern becomes quasi-steady. According to the calculations, the reason for the significant change in the layer thickness is the instability of the mixing layer whose evolution is shown in Fig. 14. The inflection point of the shock wave at the dense layer boundary is a source of perturbations irradiating concentric moderate-intensity compression waves. These waves interact with the plate surface, shock wave, and upper boundary of the channel, generating an intense background of external perturbations. External perturbations, along with the above-described internal waves in the layer, lead to the development of instability responsible for lifting of particles of the dense layer.

5. Conclusions. The wave pattern of a mixture flow upon interaction of the leading SW and a layer of small particles lying on the surface is determined by methods of numerical simulation. The wave pattern obtained is in qualitative agreement with that proposed in [1–5] on the basis of experimental studies.

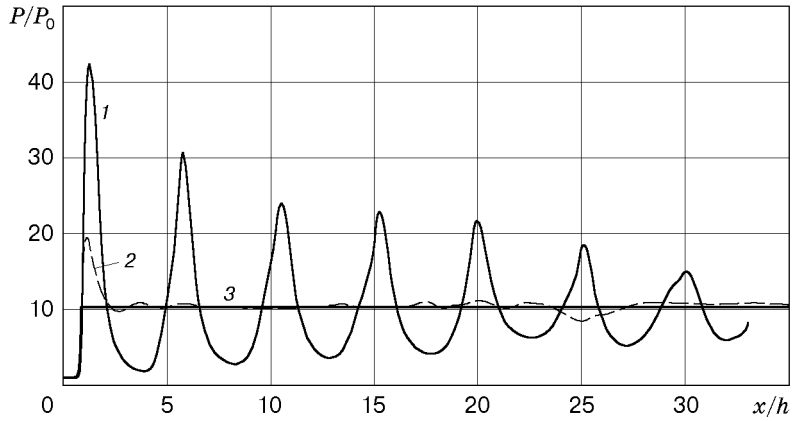

Fig. 13. Pressure distribution along the plate surface for $M_s = 3$ and $A = 3/5$ (regular reflection, curve 1), 1/3 (irregular reflection, curve 2), and 0 (pure gas, curve 3).

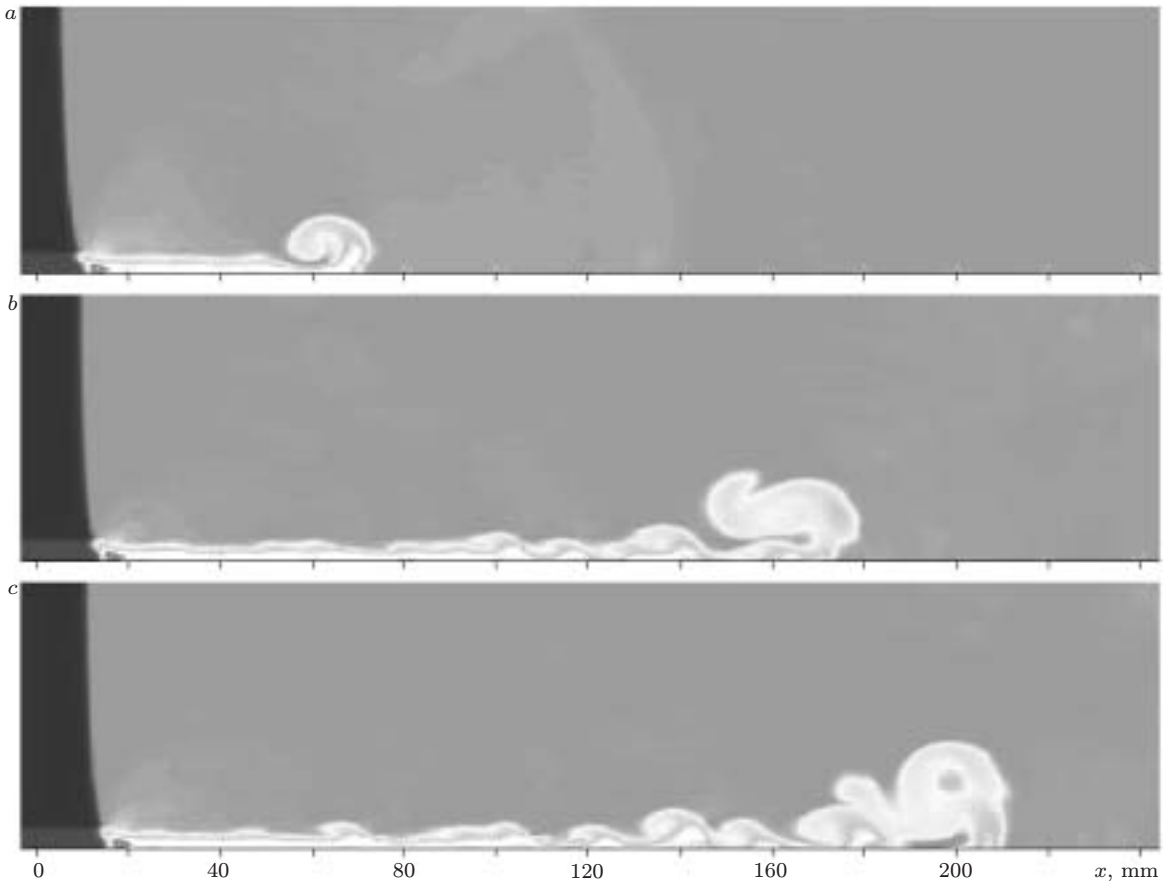

Fig. 14. Density fields for $M_s = 2$ and $A = 1/3$, and $t = 70$ (a), 330 (b), and 400 μsec (c).

The influence of SW intensity and particle concentration in the layer on the SW-amplification factor and the angle of SW deflection from the normal position is parametrically studied. It is shown that either regular or irregular regimes of reflection of the curved SW from the solid surface can be observed.

Three possible mechanisms of lifting of dust particles from the solid surface are found. The first mechanism is associated with the formation of a region with a rather high positive vertical velocity of the mixture behind the curved SW, which may lead to upward ejection of large particles. Based on the estimated distance from the SW front to the region with a positive vertical velocity, it is shown that the dependence of this distance on the

Mach number is in qualitative agreement with the empirical formula proposed in [12]. The second mechanism is conditioned by an unsteady vortex structure into which the dusty gas jet propagating in the pure gas behind the SW is "swirled." The distance from the SW to this vortex increases with time. Thus, calculations by this model cannot be used for comparison with steady calculations of the dust-lifting delay. The third possible mechanism of particle lifting is related to the Kelvin–Helmholtz instability of the shear layer, which develops in the stratified layer under the action of internal waves and external perturbations.

This work was partly supported by the International Science and Technology Center (Grant No. 612-2), Ministry of Education of the Russian Federation (Grant No. E 00-4.0-90), and Russian Foundation for Fundamental Research (Grant No. 00-01-00891).

REFERENCES

1. A. A. Borisov, A. V. Lyubimov, S. M. Kogarko, and V. P. Kozenko, "Instability of the surface of a granular medium behind sliding shock and detonation waves," *Combust. Expl. Shock Waves*, **3**, No. 1, 95–96 (1967).
2. A. A. Borisov, V. P. Kozenko, A. V. Lyubimov, and S. M. Kogarko, "Ignition of fuel powders behind shock waves," *Combust. Expl. Shock Waves*, **3**, No. 2, 192 (1967).
3. S. M. Kogarko, A. V. Lyubimov, and V. P. Kozenko, "Initiation of combustion of heterogeneous unprepared systems by shock waves," *Fiz. Goreniya Vzryva*, **5**, No. 3, 379–384 (1969).
4. A. A. Borisov, S. M. Kogarko, and A. V. Lyubimov, "Instability of the liquid surface with sliding detonation and shock waves," *Dokl. Akad. Nauk SSSR*, **164**, No. 1, 125 (1965).
5. A. A. Borisov, S. M. Kogarko, and A. V. Lyubimov, "Sliding of detonation and shock waves over liquid surfaces," *Combust. Expl. Shock Waves*, **1**, No. 4, 19–23 (1965).
6. A. V. Fedorov, N. N. Fedorova, I. A. Fedorchenko, et al., "Mathematical simulation of dynamic phenomena in mixtures of a gas and solid particles," Preprint No. 2-2001, Inst. Theor. Appl. Mech., Sib. Div., Russ. Acad. of Sci., Novosibirsk (2001).
7. A. V. Fedorov, T. A. Khmel', Yu. A. Gosteev, et al., "Mathematical simulation of steady regimes of detonation combustion of a mixture of the air–coal dust type," Report No. 7-2000, Inst. Theor. Appl. Mech., Sib. Div., Russ. Acad. of Sci., Novosibirsk (2000).
8. N. N. Yanenko, *Method of Fractional Steps for Solving Multidimensional Problems of Mathematical Physics* [in Russian], Nauka, Novosibirsk (1967).
9. V. M. Kovenya and N. N. Yanenko, *Method of Splitting in Gas-Dynamic Problems* [in Russian], Nauka, Novosibirsk (1981).
10. A. V. Borisov and N. N. Fedorova, "Numerical simulation of turbulent flows near forward-facing steps," *Thermophys. Aeromech.*, **4**, No. 1, 69–83 (1996).
11. T. Yabe, "A universal solver for hyperbolic equations for cubic-polynomial interpolation. 1. One-dimensional solver," *Comput. Phys. Comm.*, **66**, 219–232 (1991).
12. J. H. Gerrard, "An experimental investigation of the initial stages of the dispersion of dust by shock waves," *British J. Appl. Phys.*, **14**, No. 4, 186–192 (1963).